Non-Invasive Imaging of Object Behind Scattering Media via Cross-Spectrum

Xingchen Zhao, Tao Peng, Lida Zhang, M. Suhail Zubairy, Yanhua Shih, and Marlan O. Scully

***Abstract*—We develop a method based on the cross-spectrum of an intensity-modulated CW laser, which can extract a signal from an extremely noisy environment and image objects hidden in scattering media. We theoretically analyzed our scheme and performed the experiment by scanning the object placed in between two ground glass diffusers. The image of the object is retrieved by collecting the amplitudes at the modulation frequency of all the cross-spectra. Our method is non-invasive, easy-to-implement, and can work for both static and dynamic media.**

***Index Terms*—Cross-spectrum, non-invasive, Turbid media.**

I. Introduction

OPTICAL observation through scattering media is a difficult task in optics [1]–[6]. Imaging through scattering (visually opaque) media is especially challenging. The randomization of optical wavefront due to strong scattering scrambles the spatial information and smears the images obtained by light intensity measurement. A variety of strategies have been devised to image objects hidden behind the scattering media. Some methods attempt to extract the non-scattered photons, such as time-gating [7]–[10], coherence-gating [11]–[13], and rotating polarization methods [14], [15]. These techniques suffer from a low signal-to-noise ratio due to the tiny amount of non-scattered photons, which greatly limits the imaging (or penetration) depth. In addition, some gating techniques require ultrafast laser pulses, which may be devastating for living biological tissue. Some methods focus on reversing the scattering process and recovering optical input information directly from scattered photons, such as optical phase conjugation [16], [17] and transmission matrix [18]–[21]. However, they are either invasive or require interferometric and holographic measurements. Recent progress exploiting speckle correlation enables the non-invasive reconstruction of images through scattering layers with an iterative phase-retrieval algorithm [22], [23], [23]–[25]. Nevertheless, the algorithm is computationally expensive and depends on random initial guesses or prior information to achieve convergence [26]. In addition, imaging through dynamic media is still quite challenging [27]–[29]. In this case, the time-dependent mapping between input and output fields requires instant completion of the image reconstruction process to follow the motion of the medium. Although speckle correlation and shower-curtain effect have inspired an interesting attempt of looking through dynamic turbid medium in between the object and camera [30], new techniques that can image objects completely immersed in dynamic media are still highly desired.

In this letter, we report a method based on the cross-spectrum measurement from two single-pixel detectors with an intensity-modulated CW laser. The cross-spectrum technique has been mainly used to analyze the cross-correlation between two time series in the frequency domain. A CW laser with intensity modulation is commonly used in diffuse optical imaging to study the optical properties of living tissue [31]–[33]. We adopt these techniques to demonstrate a non-invasive and easy-to-implement scheme, by which the image of an object can be reconstructed not only through both static and dynamic diffusers but also under an extremely noisy environment, *i.e.*, the light intensity is much lower than detector noise. Besides, the use of CW laser makes the method more favorable in applications involving living tissues.

II. Theoretical Description of the Method

The experimental setup is shown in Fig. 1. A CW laser (633 nm, QPhotonics, QFBGLD-633-30PM) is intensity-modulated by an electro-optic modulator (EOM: Thorlabs, EO-AM-NR-C1) at frequency $f_{mod} = 1$ MHz. The modulation frequency serves as a "feature" that can be extracted later from the output light to accomplish the goal of image reconstruction. The narrow bandwidth associated with the modulated center frequency also allows circumventing the G-R noise in the detection. An objective lens (L1: Nikon, plan fluor, 10X/0.30, ∞/0, WD 17.5) is used to focus the modulated light onto the object plate (O: Thorlabs, R3L1S4N resolution test target) where the letter "1X" is transparent (height: ~ 2.3 mm; width: ~ 3.3 mm; width of transparent region: ~ 0.36 mm). The object plate is sandwiched in situ between a pair of ground glass diffusers (GGDs: Thorlabs, DG10-220) of 220 grit (average grit diameter $\bar{d}_{grit} = 53\ \mu$m). The GGD serves as the scattering medium in our experiment, as widely used in a variety of

Manuscript received May 2, 2022; accepted May 5, 2022. Date of publication May 10, 2022; date of current version May 16, 2022. This work was supported in part by the Air Force Office of Scientific Research under Grant FA9550-20-1-0366 DEF, in part by the Office of Naval Research under Grant N00014-20-1-2184, in part by Robert A. Welch Foundation under Grant A-1261, in part by National Science Foundation under Grant PHY-2013771, and in part by Qatar National Research Fund under Grant NPRP 13S-0205-200258. *(Corresponding author: Tao Peng.)*

Xingchen Zhao, Tao Peng, and M. Suhail Zubairy are with the Texas A&M University, College Station, TX 77843 USA (e-mail: toraoh007@tamu.edu; taopeng@tamu.edu; Zubairy,zubairy@physics.tamu.edu).

Lida Zhang is with Aarhus University, 8000 Aarhus C, Denmark (e-mail: zhanglida@phys.au.dk).

Yanhua Shih is with the University of Maryland, Baltimore County, MD 21250 USA (e-mail: shih@umbc.edu).

Marlan O. Scully is with Texas A&M University, College Station, TX 77843 USA, and also with Baylor University, Waco, TX 76706 USA (e-mail: scully@tamu.edu).

Digital Object Identifier 10.1109/JPHOT.2022.3173556

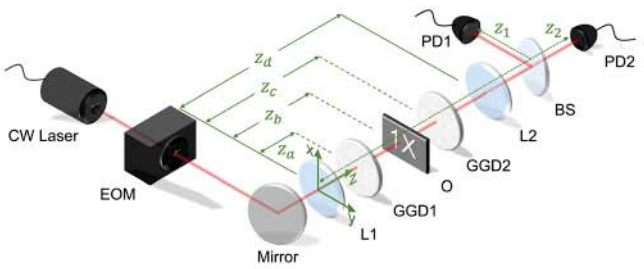

Fig. 1. Schematic of the experimental setup. We use a modulated CW laser for illumination. The object is sandwiched between two GGDs. Signal at each detector is made to be much lower than the noise level. EOM: electro-optic modulator; L: lens; GGD: ground glass diffuser; O: object; BS: beam splitter; PD: photodetector. The Cartesian coordinate is located in the center of L1 with z-axis pointing along the propagation direction of the light.

imaging scenarios [26], [34]–[36]. The focal spot is $\sim 2.7\ \mu$m in size without the GGD and is estimated to be $\sim 25\ \mu$m when GGD1 is present. A second lens (L2: $f = 150$ mm) is placed behind GDD2 to collect the scattered light. The distance between the object and each diffuser is ~ 5 mm. We note here that the distance cannot be too small due to the shower-curtain effect [30]. On the other hand, moving GGD1 nearer or further away from the object will affect the focusing condition of L1, therefore affect the resolution of the system. Moving GGD2 further away from the object will degrade the signal further collected by the two detectors, which might affect the imaging ability of the system. We also note that the target plate is put perpendicular to the beam propagation direction. When the plate is tilted at an angle, careful analysis must be taken to consider the asymmetric effect [37]. The GGDs can be either kept static or moved back and forth together by a motorized stage. The output light is split into two arms by a beam splitter (BS), which are then measured by two photodetectors (PDs: Thorlabs, PDA 10 A) respectively, where the two PDs are put at the focal plane of the lens. The data is then sent to a computer to generate images of the object. The object is scanned pixel-by-pixel with an appropriate step size to resolve the region of interest. We note here that, due to the low incident laser power ($\sim 2\ \mu W$) and scattering from the two GGDs ($\sim 75\ nW$ at the detector plane), the laser power measured at each PD is buried in the electronic and environmental noise.

We first outline a theoretical description of the cross-spectrum method [38]–[41]. As shown in Fig. 1, a Cartesian coordinate system is placed in the center of L1, with the z-axis pointing along the propagation direction of the light. A collimated incident beam of radius σ is focused by L1 with focal length f_1. The scattering centers on GGD1 will produce an electric field at distance z with the form

$$E\left(\boldsymbol{\rho}_z, z, t\right) = \frac{-ik}{2\pi} A\left(z - z_a\right) \times \int \mathrm{d}^2\boldsymbol{\rho}_{z_a} E\left(\boldsymbol{\rho}_{z_a}, z_a, t\right) R\left(\boldsymbol{\rho}_{z_a}\right) \times G\left(\boldsymbol{\rho}_z - \boldsymbol{\rho}_{z_a}; z - z_a\right), \quad (1)$$

where $\boldsymbol{\rho}_{z_a} = (x_{z_a}, y_{z_a})$ is a position vector in the in GGD1 plane, k is the wave vector, $R(\boldsymbol{\rho}_{z_a})$ describes GGD1 as a phase plate due to the scattering centers at $\boldsymbol{\rho}_{z_a}$, which imprint the random phase profile on the propagating field. We also define $A(z) = e^{ikz}/z$, $G(\alpha;\beta) = e^{ik\alpha^2/2\beta}$, and

$$E\left(\boldsymbol{\rho}_{z_a}, z_a, t\right) = E_0(t) E_a e^{-i(\nu_0 t - k z_a)} \times \exp\left\{-\frac{E_a}{2}\left(\frac{ik}{f_1} + \frac{1}{2\sigma^2}\right)\rho_{z_a}^2\right\}, \quad (2)$$

in which $E_0(t) = \sqrt{I_0 \cos 2\pi f_{mod} t}$ expresses a sinusoidal-modulation of light intensity I_0 at frequency f_{mod}, ν_0 is the frequency of the laser. $\boldsymbol{\rho}_z = (x_z, y_z)$ is the position vector in the receiver plane at distance z from L1, and

$$E_a = -\frac{ik}{2z_a} \frac{1}{1/4\sigma^2 + (ik/2)\left(1/f - 1/z_a\right)}. \quad (3)$$

The integration in (1) is performed over the illumination area on GGD1.

Since the object is scanned point by point and the light path is fixed during the scan, we can model the object as a transmission function $T(\boldsymbol{\rho}_{z_b})$ where $\boldsymbol{\rho}_{z_b} = (x_{z_b}, y_{z_b})$ is the position vector in the object plane. Upon passing through the object, being scattered by GGD2, and being collected by L2, the field at the two detectors is found to be

$$\begin{aligned} E\left(z_j, t\right) = \frac{-ik}{2\pi}\tilde{A} \iiiint \mathrm{d}^2\boldsymbol{\rho}_{z_j} \mathrm{d}^2\boldsymbol{\rho}_{z_d} \mathrm{d}^2\boldsymbol{\rho}_{z_c} \mathrm{d}^2\boldsymbol{\rho}_{z_a} \\ \times E\left(\boldsymbol{\rho}_{z_a}, z_a, t\right) R\left(\boldsymbol{\rho}_{z_a}\right) R\left(\boldsymbol{\rho}_{z_c}\right) T\left(\boldsymbol{\rho}_{z_b}\right) \\ \times G\left(\boldsymbol{\rho}_{z_c} - \boldsymbol{\rho}_{z_a}, z_c - z_a\right) G\left(\boldsymbol{\rho}_{z_d} - \boldsymbol{\rho}_{z_c}, z_d - z_c\right) \\ \times G\left(\boldsymbol{\rho}_{z_j} - \boldsymbol{\rho}_{z_d}, z_j - z_d\right) G\left(-\boldsymbol{\rho}_{z_d}, f_2\right), \end{aligned} \quad (4)$$

where $\tilde{A} = A(z_c - z_a)A(z_d - z_c)A(z_j - z_d)$, $z_j\,(j = 1, 2)$ denote the distance between the detector j and L1, f_2 is the focal length of L2, $R(\boldsymbol{\rho}_{z_c})$ describes the random phase profile due to scattering on GGD2. $G(-\boldsymbol{\rho}_{z_d}; f_2)$ is the propagation factor of L2.

The total signals measured by the two photodetectors can be expressed as

$$S\left(z_j, t\right) = I\left(z_j, t\right) + \beta_j N(t), \quad (5)$$

where $I(z_j, t) \equiv E(z_j, t)E^*(z_j, t)$ is the intensity at detector j, $N(t)$ is a white noise distribution that models all the noise due to detectors and environment, and β_j is the amplitude of the noise at detector j. It follows that the time-domain cross-correlation is given by

$$C\left(\tau\right) = \left\langle \int_0^{\mathcal{T}} \mathrm{d}t S^*\left(z_1, t\right) S\left(z_2, t + \tau\right) \right\rangle, \quad (6)$$

where $\mathcal{T}$ is the measurement time. We further assumed that the correlations between intensity and noise vanish since they are uncorrelated. On substituting from (5) into (6), we obtain

$$C\left(\tau\right) = \int_0^{\mathcal{T}} \mathrm{d}t \left\langle I\left(z_1, t\right) I\left(z_2, t + \tau\right)\right\rangle + \beta_1\beta_2 \int_0^{\mathcal{T}} \mathrm{d}t \left\langle N(t) N\left(t + \tau\right)\right\rangle. \quad (7)$$

The intensity correlation in the first term of (7) can be expressed as

$$\begin{aligned}&\langle I(z_1,t)\, I(z_2,t+\tau)\rangle\\&= \langle E(z_1,t)\, E^*(z_1,t)\, E(z_2,t+\tau)\, E^*(z_2,t+\tau)\rangle \end{aligned} \tag{8}$$

where $E(z_j,t)$ $(j=1,2)$ is given by (4). Since the scattering centers are independent of each other and satisfy Gaussian statistics, the random phase term $R(\rho_{z_i})$ obeys

$$\left\langle R\left(\rho_{z_i}\right) R^*\left(\rho'_{z_i}\right)\right\rangle = \delta\left(\rho_{z_i}-\rho'_{z_i}\right) \tag{9}$$

and

$$\begin{aligned}&\left\langle R\left(\rho_{z_i}\right) R^*\left(\rho'_{z_i}\right) R\left(\rho''_{z_i}\right) R^*\left(\rho'''_{z_i}\right)\right\rangle\\&= \delta\left(\rho_{z_i}-\rho'_{z_i}\right)\delta\left(\rho''_{z_i}-\rho'''_{z_i}\right)+\delta\left(\rho_{z_i}-\rho'''_{z_i}\right)\delta\left(\rho'_{z_i}-\rho''_{z_i}\right)\end{aligned} \tag{10}$$

where $i=a,c$ and $\delta(\rho-\rho')$ is the delta function. The second term in (7) is given by [42]

$$\int_0^{\mathcal{T}} \mathrm{d}t\, \langle N(t)N(t+\tau)\rangle = \delta(\tau). \tag{11}$$

Upon substituting (2), (4), and (8) – (11) into (7), we obtain after carrying out the integrations

$$C(\tau) \propto \mathcal{T}\left|T\left(\rho_{z_b}\right)\right|^4 \cos\left(2\pi f_{mod}\tau\right)+\beta_1\beta_2\delta(\tau). \tag{12}$$

It follows from (12) that the cross-correlation is

$$\begin{aligned}\Gamma\left(\rho_{z_b};\omega\right) &= \int_{-\infty}^{\infty} C(\tau)\, e^{-i\omega\tau}\mathrm{d}\tau\\&= \Gamma_0\mathcal{T}\left|T\left(\rho_{z_b}\right)\right|^4\delta\left(\omega-2\pi f_{mod}\right)+\beta_1\beta_2,\end{aligned} \tag{13}$$

where

$$\Gamma_0 = \left(\frac{4\pi^2}{k^2}\right)^2 \frac{(\pi\sigma^2)^2\left|\tilde{A}\right|^4 I_0^2}{f_{mod}}. \tag{14}$$

The cross-spectrum is a sum of frequency peak signal multiplied by $|T(\rho_{z_b})|^2$ and uniform noise background. Note the object ("1X") can be represented by $|T(\rho_{z_b})|^2$. Scanning the object and recording $S_1(t)$ and $S_2(t)$ at every position ρ_{z_b}, we can calculate the cross-spectrum as a function of the position. A heat map of $\Gamma(\rho_{z_b};\omega=2\pi f_{mod})$ will produce an image of the object, because $|T(\rho_{z_b})|^4$ serves as a "mask" that modulates the amplitudes of the cross-spectrum from position to position as indicated in (13), and the shape of the object is finally encoded in $\Gamma(\rho_{z_b};\omega=2\pi f_{mod})$. Furthermore, the larger the integration time $\mathcal{T}$ is, the greater the amplitude of the frequency peak will be; while, the noise is independent of $\mathcal{T}$. This suggests that, by increasing $\mathcal{T}$, the signal-to-noise ratio can be enhanced. Therefore, even though the output signal may undergo strongly scattering and is below the noise level of the detectors, this method can still reconstruct the image of the target.

III. Experimental Results

We firstly show that how our method can distinguish the signal by performing the cross-spectrum. As shown in Fig. 2, we compare two cases when a point-like object is made opaque or transparent. For each case, we record the intensity at each detector for 500 μs, where the average intensity is indicated by the red solid line. We then perform Fourier transform to each set of data, and calculate the cross-spectrum of the two signals. For efficient numerical computation of cross-spectrum, we exploit the relation $\mathcal{F}\{f\star g\}=\overline{\mathcal{F}\{f\}}\cdot\mathcal{F}\{g\}$, where $\mathcal{F}$ denotes Fourier transform, $f\star g$ denotes the cross-correlation of two functions f and g. The two Fourier transform from two detectors are then used to produce the cross-spectrum. As shown in Fig. (2), since the signal intensity is much below the noise level of the detectors, the intensity cannot distinguish whether the point-like object is opaque or transparent. and Fourier transform are not able to distinguish However, the cross-spectrum shows significantly different amplitudes at f_{mod} for the opaque and transparent cases. Therefore, for an 2D object, the values of the cross-spectrum amplitude at different locations can produce an image of the object.

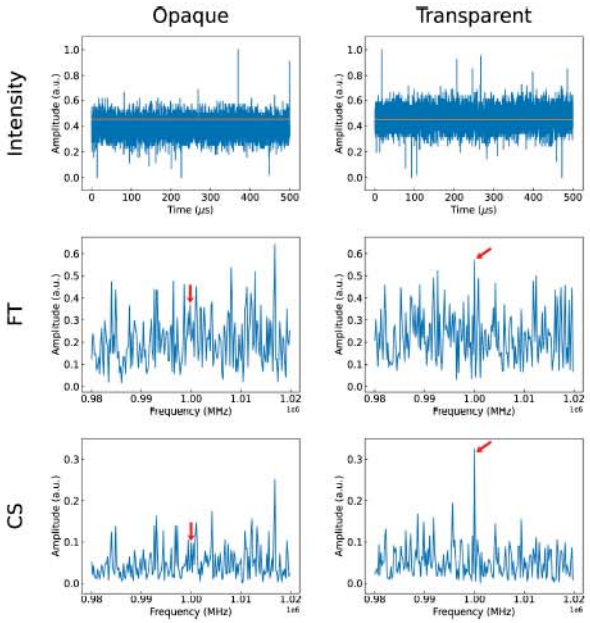

Fig. 2. Comparison of a single point when light is blocked (left column) and transmitted (right column). From top to bottom: Intensity recorded at one detector; Fourier spectrum (FT) of single detector signal; Cross-spectrum (CS) of signals from both detectors. The modulation frequency f_{mod} is marked in red arrow.

TABLE I
Visibility for Different Diffuser States

Diffuser State	Intensity	Cross-spectrum
No diffuser (ND)	0.725	0.967
Static diffuser (SD)	0.032	0.451
Dynamic diffuser (DD)	0.031	0.558

To demonstrate that our method works experimentally for both static and dynamic scattering media, we then perform the measurements under three situations: 1. imaging without the diffuser (no diffuser, ND); 2. the object is sandwiched between two static diffusers (SDs); and 3. the two diffusers are moved back and forth together by a motorized stage (dynamic diffusers, DDs). The stage moves at a random speed with upper limits of the speed and acceleration set to be 500 mm/s and 1500 mm/s^2, respectively. The full range is 1.5 cm. The object has the letter "1X" being transparent and other regions being opaque. For all three cases, data are collected by an oscilloscope with a fixed

TABLE II
VISIBILITY OF DIFFERENT ACQUISITION TIME FOR STATIC AND DYNAMIC DIFFUSER STATES

Acquisition time	Static diffuser (SD)		Dynamic diffuser (DD)	
	Intensity	Cross-spectrum	Intensity	Cross-spectrum
50 μs	0.027 ± 0.004	0.135 ± 0.009	0.035 ± 0.005	0.190 ± 0.004
100 μs	0.033 ± 0.004	0.332 ± 0.001	0.030 ± 0.002	0.305 ± 0.004
500 μs	0.034 ± 0.003	0.466 ± 0.008	0.048 ± 0.004	0.560 ± 0.002

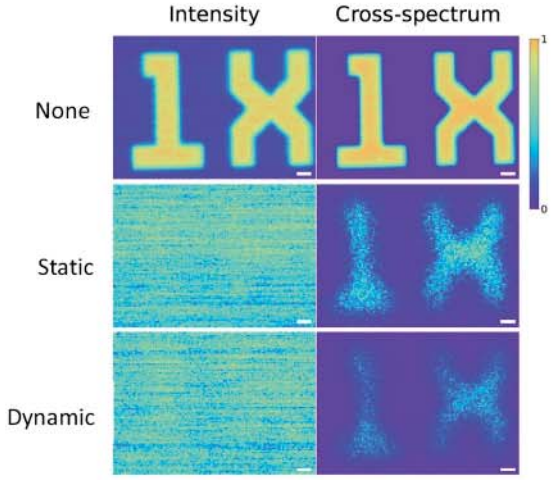

Fig. 3. Raster-scan images for an object with the letter "1X" being transparent and other regions being opaque. Cross-spectrum images are generated by plotting $\Gamma(\rho_b, \omega = 2\pi f_{mod})$ (see (13)). Scale bar, 40 pixels. None: no diffuser. Scale bar: 10 pixels (0.25 mm).

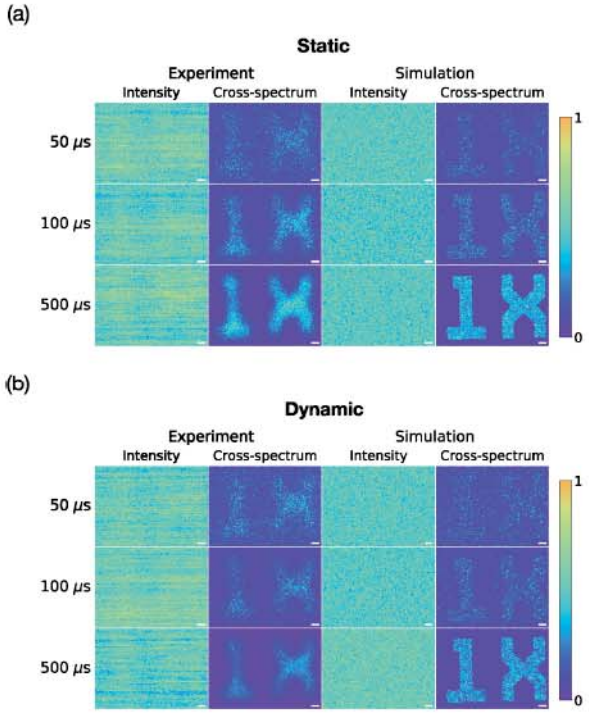

Fig. 4. Raster-scan images and simulations for different acquisition time with (a) static diffusers and (b) dynamic diffusers. Scale bar: 10 pixels (0.25 mm).

sample rate at 2 GHz. At each position, 1 million data points are taken to calculate the cross-spectrum, corresponding to 500 μs integration time which ensures a strong cross-correlation signal. The whole image contains 100×140 pixels (number of steps scanned) with the pixel size (scanning step size) of 25 μm.

The main experimental result' is shown in Fig. 3, of which the pixel values v are normalized by $\tilde{v} = (v - v_{min})/(v_{max} - v_{min})$. In the first column, we directly plot the intensity measured by the detectors; while, in the second column, we plot $\Gamma(\rho_b, 2\pi f_{mod})$. The first row shows ND images. The second and third row list images obtained with SD and DD, respectively. We summarize the visibility of images in Table I, which is calculated by $V = (\bar{\tilde{v}}_s - \bar{\tilde{v}}_b)/(\bar{\tilde{v}}_s + \bar{\tilde{v}}_b)$, where $\bar{\tilde{v}}_s$ and $\bar{\tilde{v}}_b$ are the average pixel values of signal ("1X" region) and background, respectively. As shown in Fig. 3, in both SD and DD cases, when the scattering media is present, the recorded intensity does not show any image in either case, the extremely low visibility is a sign that our signal is truly at the noise level of the detectors. On the other hand, in both cases, the images are still retrieved using the cross-spectrum technique with high visibility. The results suggest that the cross-spectrum method can image an object hidden behind both static and dynamic scattering media. We also notice that the visibility of the cross-spectrum image is higher than the intensity image even though there is no diffuser (ND), which suggests cross-spectrum is also an effective way to enhance the signal-to-noise ratio when the scattering media is absent.

To further test our method, we also compare the measured images from different acquisition time (50 μs, 100 μs, and 500 μs) with the same sample rate. The incident intensity of light is fixed for the static and dynamic diffusers. Simulation is also performed for the intensity and cross-spectrum based on (5) and (13), respectively, to compare with the experimental results. The results are shown in Fig. 4, the corresponding visibility of the experimental results are listed in Table II. It can be seen that, in general, the longer the integration time is, the higher visibility one can achieve for both static and dynamic diffusers. This means we can obtain a clear image at the expense of a long acquisition time. We note that the visibility of the recorded intensity image is kept extremely low even when one increases the acquisition time up to 10 times. Nevertheless, the cross-spectrum image becomes more and more clear. The visibility also increases much faster than that of the intensity measurement when increasing the acquisition time. We point out that the fundamental limit of imaging speed is the acquisition length, which is on the order of 100 μs for the current setup but can be, in principle, orders faster with higher modulation frequency and higher sample rate (GHz range laser modulation speed and detection). The raster scan speed can also be much improved if, for instance, a 2D galvo-resonant scanner is integrated into the system.

IV. SUMMARY

In conclusion, we have developed a cross-spectrum method to extract a weak optical signal from the extremely noisy

background and image objects hidden behind scattering media. The major advantage of this scheme is that it uses a CW laser in a non-invasive manner which would be easy to implement and bio-tissue friendly. It is effective for both static and dynamic media, making it adaptive in most application situations with various scattering levels, as long as the power of the incident light and the integration time is sufficient so that the cross-spectrum signal overcomes the noise level. With the fast acquisition time with current technology, our scheme paves the way for efficient imaging in previously inaccessible scenarios.

REFERENCES

[1] R. E. Meyers, K. S. Deacon, and Y. Shih, "Turbulence-free ghost imaging," *Appl. Phys. Lett.*, vol. 98, no. 11, 2011, Art. no. 111115.

[2] A. P. Mosk, A. Lagendijk, G. Lerosey, and M. Fink, "Controlling waves in space and time for imaging and focusing in complex media," *Nature Photon.*, vol. 6, no. 5, pp. 283–292, 2012.

[3] J. Bertolotti, E. G. Van Putten, C. Blum, A. Lagendijk, W. L. Vos, and A. P. Mosk, "Non-invasive imaging through opaque scattering layers," *Nature*, vol. 491, no. 7423, pp. 232–234, 2012.

[4] S. Rotter and S. Gigan, "Light fields in complex media: Mesoscopic scattering meets wave control," *Rev. Mod. Phys.*, vol. 89, no. 1, 2017, Art. no. 015005.

[5] V. Ntziachristos, "Going deeper than microscopy: The optical imaging frontier in Biology," *Nature Methods*, vol. 7, no. 8, pp. 603–614, 2010.

[6] A. Bhattacharjee, S. Aarav, H. Wanare, and A. K. Jha, "Controlling propagation of spatial coherence for enhanced imaging through scattering media," *Phys. Rev. A*, vol. 101, no. 4, 2020, Art. no. 0 43839.

[7] L. Wang, P. Ho, C. Liu, G. Zhang, and R. Alfano, "Ballistic 2-D imaging through scattering walls using an ultrafast optical Kerr gate," *Science*, vol. 253, no. 5021, pp. 769–771, 1991.

[8] M. R. Hee, J. A. Izatt, J. M. Jacobson, J. G. Fujimoto, and E. A. Swanson, "Femtosecond transillumination optical coherence tomography," *Opt. Lett.*, vol. 18, no. 12, pp. 950–952, 1993.

[9] B. Das, K. Yoo, and R. Alfano, "Ultrafast time-gated imaging in thick tissues: A step toward optical mammography," *Opt. Lett.*, vol. 18, no. 13, pp. 1092–1094, 1993.

[10] F. Liu, K. Yoo, and R. Alfano, "Transmitted photon intensity through biological tissues within various time windows," *Opt. Lett.*, vol. 19, no. 10, pp. 740–742, 1994.

[11] N. H. Abramson and K. G. Spears, "Single pulse light-in-flight recording by holography," *Appl. Opt.*, vol. 28, no. 10, pp. 1834–1841, 1989.

[12] H. Chen, Y. Chen, D. Dilworth, E. Leith, J. Lopez, and J. Valdmanis, "Two-dimensional imaging through diffusing media using 150-fs gated electronic holography techniques," *Opt. Lett.*, vol. 16, no. 7, pp. 487–489, 1991.

[13] E. Leith *et al.*, "Electronic holography and speckle methods for imaging through tissue using femtosecond gated pulses," *Appl. Opt.*, vol. 30, no. 29, pp. 4204–4210, 1991.

[14] H. Ramachandran and A. Narayanan, "Two-dimensional imaging through turbid media using a continuous wave light source," *Opt. Commun.*, vol. 154, no. 5–6, pp. 255–260, 1998.

[15] O. Emile, F. Bretenaker, and A. Le Floch, "Rotating polarization imaging in turbid media," *Opt. Lett.*, vol. 21, no. 20, pp. 1706–1708, 1996.

[16] M. Cui and C. Yang, "Implementation of a digital optical phase conjugation system and its application to study the robustness of turbidity suppression by phase conjugation," *Opt. Exp.*, vol. 18, no. 4, pp. 3444–3455, 2010.

[17] Z. Yaqoob, D. Psaltis, M. S. Feld, and C. Yang, "Optical phase conjugation for turbidity suppression in biological samples," *Nature Photon.*, vol. 2, no. 2, pp. 110–115, 2008.

[18] S. Popoff, G. Lerosey, R. Carminati, M. Fink, A. Boccara, and S. Gigan, "Measuring the transmission matrix in optics: An approach to the study and control of light propagation in disordered media," *Phy. Rev. Lett.*, vol. 104, no. 10, 2010, Art. no. 100601.

[19] J. Yoon, K. Lee, J. Park, and Y. Park, "Measuring optical transmission matrices by wavefront shaping," *Opt. Exp.*, vol. 23, no. 8, pp. 10158–10167, 2015.

[20] M. Mounaix, H. Defienne, and S. Gigan, "Deterministic light focusing in space and time through multiple scattering media with a time-resolved transmission matrix approach," *Phys. Rev. A*, vol. 94, no. 4, 2016, Art. no. 041802.

[21] H. B. de Aguiar, S. Gigan, and S. Brasselet, "Enhanced nonlinear imaging through scattering media using transmission-matrix-based wave-front shaping," *Phys. Rev. A*, vol. 94, no. 4, 2016, Art. no. 043830.

[22] O. Katz, P. Heidmann, M. Fink, and S. Gigan, "Non-invasive single-shot imaging through scattering layers and around corners via speckle correlations," *Nature Photon.*, vol. 8, no. 10, pp. 784–790, 2014.

[23] J. A. Newman, Q. Luo, and K. J. Webb, "Imaging hidden objects with spatial speckle intensity correlations over object position," *Phys. Rev. Lett.*, vol. 116, no. 7, 2016, Art. no. 073902.

[24] K. J. Webb and Q. Luo, "Theory of speckle intensity correlations over object position in a heavily scattering random medium," *Phys. Rev. A*, vol. 101, no. 6, 2020, Art. no. 063827.

[25] Q. Luo and K. J. Webb, "Parametrization of speckle intensity correlations over object position for coherent sensing and imaging in heavily scattering random media," *Phys. Rev. Res.*, vol. 2, no. 3, 2020, Art. no. 033148.

[26] T. Wu, O. Katz, X. Shao, and S. Gigan, "Single-shot diffraction-limited imaging through scattering layers via bispectrum analysis," *Opt. Lett.*, vol. 41, no. 21, pp. 5003–5006, 2016.

[27] Y. Yuan and H. Chen, "Non-invasive dynamic or wide-field imaging through opaque layers and around corners," 2017, *arXiv:1712.08576*.

[28] Y. Sun, J. Shi, L. Sun, J. Fan, and G. Zeng, "Image reconstruction through dynamic scattering media based on deep learning," *Opt. Exp.*, vol. 27, no. 11, pp. 16032–16046, 2019.

[29] H. Ruan, Y. Liu, J. Xu, Y. Huang, and C. Yang, "Fluorescence imaging through dynamic scattering media with speckle-encoded ultrasound-modulated light correlation," *Nature Photon.*, vol. 14, no. 8, pp. 511–516, 2020.

[30] E. Edrei and G. Scarcelli, "Optical imaging through dynamic turbid media using the Fourier-domain shower-curtain effect," *Optica*, vol. 3, no. 1, pp. 71–74, 2016.

[31] J. B. Fishkin, E. Gratton, and W. W. Mantulin, "Diffusion of intensity modulated near-infrared light in turbid media," *Proc. SPIE*, vol. 1431, 1991, pp. 122–135.

[32] B. J. Tromberg, L. O. Svaasand, T.-T. Tsay, R. C. Haskell, and M. W. Berns, "Optical property measurements in turbid media using frequency-domain photon migration," *Proc. SPIE*, vol. 1525, 1991, pp. 52–58.

[33] T. D. O'Sullivan, A. E. Cerussi, B. J. Tromberg, and D. J. Cuccia, "Diffuse optical imaging using spatially and temporally modulated light," *J. Biomed. Opt.*, vol. 17, no. 7, 2012, Art. no. 071311.

[34] Y. Suzuki and L. V. Wang, "Frequency-swept time-reversed ultrasonically encoded optical focusing," *Appl. Phys. Lett.*, vol. 105, no. 19, 2014, Art. no. 191108.

[35] A. Roy, R. K. Singh, and M. M. Brundavanam, "Analysis of polarization speckle for imaging through random birefringent scatterer," *Appl. Phys. Lett.*, vol. 109, no. 20, 2016, Art. no. 201108.

[36] O. Tzang, E. Niv, S. Singh, S. Labouesse, G. Myatt, and R. Piestun, "Wavefront shaping in complex media with a 350 KHz modulator via a 1D-to-2D transform," *Nature Photon.*, vol. 13, no. 11, pp. 788–793, 2019.

[37] A. Sriram, C. Wu, R. Lee, and C. C. Davis, "Exploiting forward-scattering asymmetry in imaging and surface profile measurements through scattering media," *OSA Continuum*, vol. 3, no. 3, pp. 410–419, 2020.

[38] L. E. Estes, L. M. Narducci, and R. A. Tuft, "Scattering of light from a rotating ground glass," *J. Opt. Soc. Amer.*, vol. 61, no. 10, pp. 1301–1306, 1971.

[39] J. Churnside, "Speckle from a rotating diffuse object," *J. Opt. Soc. Amer.*, vol. 72, no. 11, pp. 1464–1469, 1982.

[40] J. W. Goodman, *Speckle Phenomena in Optics: Theory and Applications*. Greenwood Village, CO, USA: Roberts and Company Publishers, 2007.

[41] J. T. Foley and M. Zubairy, "The directionality of Gaussian Schell-model beams," *Opt. Commun.*, vol. 26, no. 3, pp. 297–300, 1978.

[42] J. J. Shynk, *Probability, Random Variables, and Random Processes: Theory and Signal Processing Applications*. Hoboken, NJ, USA: Wiley, 2012.